Mobile based Human Identification using Forehead Creases: Application and Assessment under COVID-19 Masked Face Scenarios

Anonymous WACV submission

Paper ID 1242

Abstract

In the COVID-19 situation, face masks have become an essential part of our daily life. As mask occludes most of the prominent facial characteristics, it brings new challenges to the existing facial recognition systems. This paper presents an idea to consider forehead creases (under surprise facial expression) as a new biometric modality to authenticate mask wearing faces. The forehead biometrics utilizes the creases and textural skin patterns appearing due to voluntary contraction of the forehead region as features. The proposed framework is an efficient and generalizable deep learning framework for forehead recognition. To achieve this goal, face-selfie images are collected using smartphone's frontal camera in an unconstrained environment having variety of indoor/outdoor realistic environments. Acquired forehead images are first subjected to segmentation model that results in rectangular ROI's. A set of convolutional feature maps are subsequently obtained using a backbone network. To induce discriminative feature learning, the primary embeddings are enriched using dual attention network (DANet). The attention empowered embedddings are then optimized using large margin cosine loss followed by a focal loss to update weights for inducting robust training and better feature discriminating capabilities. Our system is an end-to-end and few-shot thus, it is very efficient in terms of memory requirements and recognition rate. Besides, we present a forehead image dataset that has been recorded in two sessions from 247 subjects containing a total of 4,964 selfie-face mask images. To the best of our knowledge, this is the first to date mobile based forehead dataset and is being made available along with mobile application in the public domain. The proposed system has achieved high performance results in both closed set i.e., CRR of 99.08% and EER of 0.44% and open set matching i.e., CRR: 97.84%*, EER:* 12.40% *which justifies the significance of using forehead as a biometric modality.*

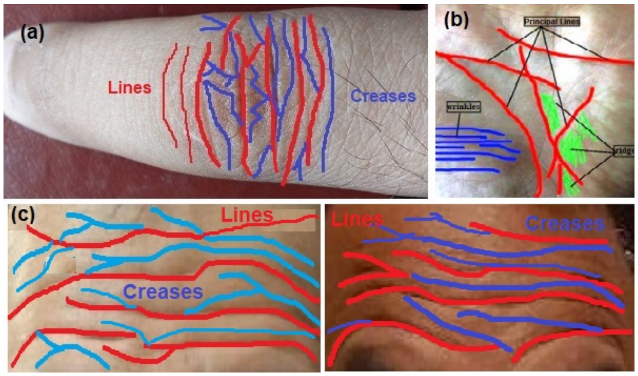

Figure 1: Examples images of (a) finger knuckle print, and (b) palmprint are showing similar line and crease-patterns to (c) forehead creases that indicate the addition of forehead patterns for biometric recognition could address the challenges in masked face scenarios.

1. Introduction

The most successfully adopted biometrics to unlock smartphones are face selfie (introduced with Android 4.0), iris scanner (introduced with Galaxy Note 7) and fingerprint touch (introduced with Apple's iPhone 5s) mechanisms [2]. Additionally, commercial solutions for mobile biometric recognition based on inbuilt smartphone sensors are already available. Since, the COVID-19 can spread through contact and contaminated surfaces, face, iris, voice, and fingerprint based classical biometric methods undergone serious challenges: 1) accessing face authentication when a major part of the face is hidden by a mask can prevent us from unlocking our smartphone, 2) touching fingerprint scanner might increase the possibility of contamination, thereby triggering infectious diseases. 3) iris authentication seems more dependent on high quality images. Unlike face recognition [16], periocular [1] and voice [15] may be utilized as alternate recognition systems, however, they are not very reliable when substantial portions of the face are occluded. Some recent studies have shown consequences of face coverings upon the quality of speech [5]. Face mask and low quality images might present obstruction to reliable seg-

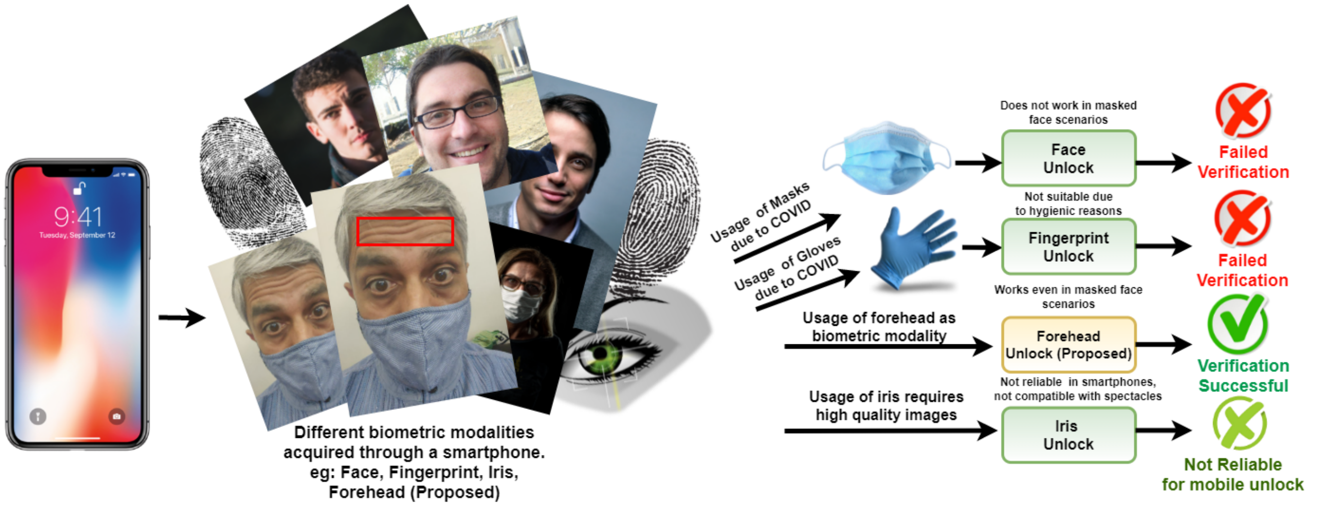
9:41
Tuesday, September 12
Different biometric modalities acquired through a smartphone. eg: Face, Fingerprint, Iris, Forehead (Proposed)
Usage of Masks due to COVID
Usage of Gloves due to COVID
Usage of forehead as biometric modality
Usage of iris requires high quality images
Does not work in masked face scenarios
Face Unlock
Failed Verification
Not suitable due to hygienic reasons
Fingerprint Unlock
Failed Verification
Works even in masked face scenarios
Forehead Unlock (Proposed)
Verification Successful
Not reliable in smartphones, not compatible with spectacles
Iris Unlock
Not Reliable for mobile unlock

Figure 2: Overview of challenges for reliable biometric recognition and suitability of forehead crease patterns for smartphone authentication under COVID-19 masked face scenarios.

mentation of periocular region [17]. Due to aforementioned problems, there is a reinforced requirement to look for alternate biometric identifiers which could be utilized in the COVID-19 era, in particular with regards to the wearing of face masks. Aiming towards, our work investigates forehead creases (under facial expressions) as a biometric trait that can give competitive results as compared to face and periocular in the COVID-19 era when masks must be worn by everyone and where touchable interactions must preferably be avoided.

Related Work and Challenges Before turning to the technical description of our approach, we first provide background on prior studies in forehead recognition. Since, forehead crease patterns to the best of our knowledge is a very less explored biometric modality in the literature so far. The first ever work in forehead recognition was presented by [11], but the purpose is not useful for smartphone based applications. Their system acquired forehead images using a complex imaging system based on near-infrared laser scanning. Also, their setup is cope up with hygienic concerns, sensor surface noise and user inconvenience as one has to maintain a head posture and then put head on a surface for data collection, thus not suitable in COVID-19 applications. The approach detailed in this reference is a baseline work without much optimization of forehead patterns for smartphone based user recognition. It is worth mentioning that acquisition of forehead image using smartphone offers higher user convenience, and contactless imaging aspects. In such forehead images, skin creases and lines are the major source of information which are observed to be distinct and permanent for each individuals due to the differences of frontal bone morphology, and thickness of the skin tissues [12].

We assume and hypothesise that forehead creases have similar image properties to finger knuckle print [7] and palmprint [13] which are well established traits in establishing human identities. Figure 1 indicates the anatomical view of forehead patterns that has full potential to be considered as biometric modality as similar to palmprint and knuckleprint. However, the uniqueness of such wavy and horizontal lines of varying thickness is not fully sufficient to establish the personal identity in non-cooperative conditions or recognition at a distance. Moreover, contactless imaging via smartphone often introduces deformation of forehead patterns due to pose, scale and illumination, thus a full potential from the forehead biometrics is yet to be realized. Figure 2 illustrates the need of forehead based smartphone recognition systems when other well known biometrics are causing serious challenges due to facial masks and urgent hygienic concerns.

1.1. Our Work and Contribution

To the best of authors knowledge, this is the first work motivated to advance the smartphone based forehead recognition capabilities in masked face scenarios, especially in the context of COVID-19 pandemic. Our mobile application requires bare minimum hardware and memory requirements, i.e., an android smartphone device and 5 MB of space, thus there is an increased scope of reproducibility. Our dataset is composed of $4,940$ image examples taken in two different sessions where we have 20 image poses per 247 subjects. However, we make an assumption that the mobile app user is cooperative during contactless forehead imaging and such cooperation is often expected from fingerprint, iris or other contactless biometrics systems.

Contributions: Our work describes a complete forehead

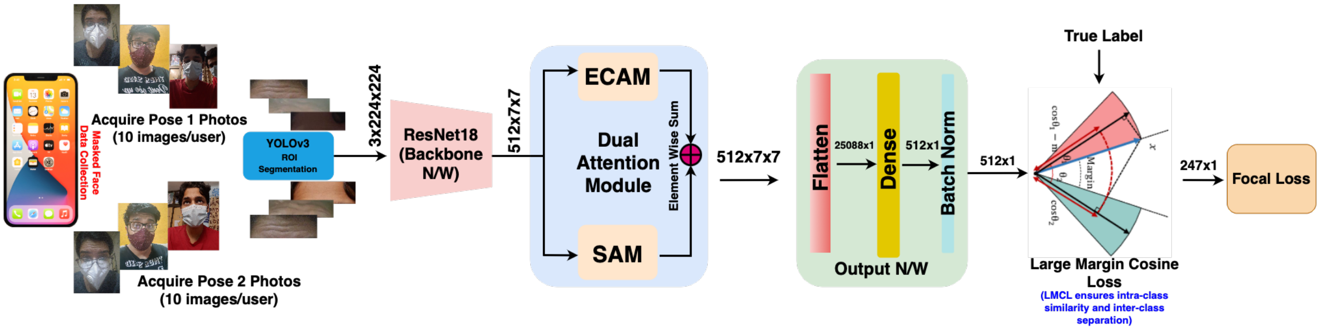

Figure 3: Block diagram of the proposed forehead recognition network assisted with dual attention network. The network performs discriminative feature learning in cosine space that has richer embedding representation than state-of-art networks.

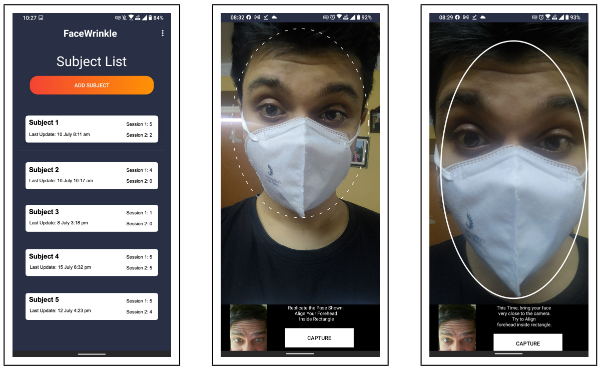

FaceWrinkle

Subject List

ADD SUBJECT

Subject 1 Session 1: 5
Last Update: 10 July 8:11 am Session 2: 2

Subject 2 Session 1: 4
Last Update: 10 July 10:17 am Session 2: 0

Subject 3 Session 1: 1
Last Update: 8 July 3:18 pm Session 2: 0

Subject 4 Session 1: 5
Last Update: 15 July 6:32 pm Session 2: 5

Subject 5 Session 1: 5
Last Update: 12 July 4:23 pm Session 2: 4

Replicate the Pose Shown.
Align Your Forehead
Inside Rectangle

CAPTURE

This Time, bring your face
very close to the camera.
Try to Align
forehead inside rectangle.

CAPTURE

(a) (b) (c)

Figure 4: Data collection app. (a) interface, (b) Pose-1 from a fixed distance, (c) Pose-2 with camera close to face.

segmentation and recognition pipeline using an end-to-end deep metric learning approach whose detailed architecture is depicted in Figure 3. To this end, the following main aspects are considered: 1) how to achieve a consistent forehead localization under multiple spatial scales, varying poses, occlusion, and illumination? 2) how to obtain a computationally efficient yet effective baseline CNN model for mobile based forehead recognition? 3) how to take advantage of metric learning domain to improve the recognition performance in data scarce conditions?

Contact-less data collection with varying scale, pose, occlusion and discrete crease patterns raise several challenges for forehead RoI segmentation and recognition. This paper introduces a challenging masked face dataset and attempts to work on the aforementioned challenges. The key contributions of this paper are summarised in the following points:

1. To the best of our knowledge, this is the first biometric human recognition approach with forehead-images.
2. We presents deep metric learning using large margin cosine loss that is highly optimised for extracting discriminative features for the forehead recognition.
3. Incorporating a dual attention mechanism that considers spatial attention to learn semantic regularities and channel attention to compute correlation between all the channels independently.
4. Devised a smart data acquisition strategy using front camera of mobile devices. The samples are acquired remotely in two sessions, our android application facilitates the process by providing on screen GUI.
5. Developed a forehead-image database, consisting of 4,940 selfie masked faces and corresponding cropped ROI's captured from 247 subjects.
6. Similar to face recognition methods, the proposed framework has been extended to provide open-set recognition performance.

We demonstrate forehead-image recognition performance using standard eveluation measures: correct recognition rate (CRR), equal error rate (EER), decidabilty index (DI) along with receiving operating characteristic (ROC) curve. Besides, we used jaccard index (Intersection Over Union), precision and recall to measure the performance of RoI segmentation.

The rest of the paper is structured into four main sections. Section II describes the image acquisition setup via mobile app and detail about the dataset. Section III presents the methodology of our approach and includes the details of the network and training considered in this work. Section IV details about experiments, matching protocol employed for performance evaluation. Key findings and discussions are summarized in the last section.

2. Forehead Image Acquisition

We use a non-contact and remote imaging setup to acquire masked face samples in non-uniform lighting, and changing background conditions. Keeping in mind the significance of isolation/ social distancing, a special android application is developed to ease the smartphone based data-acquisition process in a remote manner. The data is taken in two sessions, wherein each session a subject is required to provide 5 photographs of the two poses. The above two poses are taken into consideration to account for the variance due to distance. The Android app GUI first allows users to bring their faces into a guided bounding box to keep

Subjects	Accuracy (%)	Precision	Recall	IOU
15	72.80	0.76	0.85	0.78
30	73.11	0.77	0.85	0.79
45	73.84	0.77	0.86	0.79

Table 1: Segmentation performance under different training datasets

consistency in face postures across the dataset, as shown in Fig 4 (b) and Fig 4 (c). Pose 1 is taken in first session such that the user maintains a fixed distance between the camera and the phone, while pose 2 (in second session) requests the user to close the gap between the camera and the phone. The user has to make a surprise reaction and lift their eyebrows exactly like shown in Fig 4 (b) & (c), for getting the forehead wrinkle patterns to be visible. Most importantly, session 2 photographs are taken after a minimum time gap of 1 day to ensure the temporal stability of forehead patterns. In this way, each subject has provided 20 $(5 samples \times 2 poses \times 2 sessions)$ photographs. The mobile application is designed as a client-server model, thus all the data is collected remotely in an unconstrained environment.

3. Proposed Approach

In this section, we first summarize the whole pipeline of a forehead recognition system and then elaborate on the details of the proposed approach, including segmentation and backbone network with dual attention mechanism assisted and simple yet effective large margin cosine loss [19]. We argue that rather than designing and training new CNNs for forehead recognition, using CNNs whose architectures have already been proven to be successful in large-scale datasets, can yield good performance without tedious architecture steps. The pipeline of a complete forehead recognition system is illustrated in Figure 3, including forehead RoI segmentation, feature extraction while focusing on discriminative patterns and matching. Without loss of generality, we use Yolo v3 for segmentation task, ResNet18 is chosen as our backbone network driven by dual attention (DANet) ([20], [4]) and LMCL [19] is used as loss function. However, there is a need for using attention mechanisms to further enhance the feature discrimination in both spatial and channel dimensions. The dual attention mechanism is incorporated into the backbone network to discover more discriminative feature representation for forehead images than the standard feature learning.

3.1. Extracting the Region of Interest

Some of the inherent problems in our non-ideal forehead dataset, which we have mainly focused are: changing face postures, blurred boundaries, complex backgrounds, illumination variation and occlusions by hairs, glasses, and dots worn on foreheads. In Fig 6, some of challenging images containing occlusion, illumination etc., are highlighted. Since the data was taken remotely due to the lockdown restrictions, many users were not able to provide good quality face data. After locating the raw forehead regions via app GUI, one can use any state-of-the-art detection networks for RoI segmentation, we deployed a simple yet effective pre-trained YOLOv3 model [14] (which originally was trained on Imagenet) on around 600 raw forehead images from 30 subjects. Using the trained weights from YOLOv3 model, we obtained bounding boxes over rest of the $4,340$ forehead images from 217 subjects. Each subject has a maximum of 20 images, few has less than 20 images because all the defections whose confidence score is less than 0.6 were dropped. The state-of-the-art evaluation parameters like jaccard index, accuracy, precision, and recall are computed for all the studied cases and are shown in Fig 5 & Fig 7. The mean values of these metrics on IOU thresholds ranging from 0.1 to 0.99 with a step size of 0.01 are displayed in Table 1. Figure 6 (a) and (b) show a few challenging masked face images and corresponding forehead ROI's where our network performs well, while Figure 6 (c) and (d) shows examples of forehead images suffered from various type of noise factors (occlusion, illumination, glasses etc) and corresponding poor quality segmentation results. Figure 7 shows the precision–recall graph for different training data sets, where bars and dashed lines represent precision and recall, respectively. It can be observed that up to IOU ≤ 0.7, the precision and recall of the segmentation network over all the training data sets remains very high and they decrease significantly after IOU = 0.8.

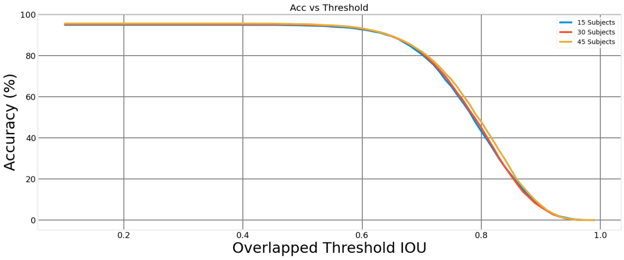

Figure 5: Forehead segmentation accuracy on different training datasets with respect to threshold on IOU

3.2. Backbone Network

Given a cropped forehead image $x^{(i)} \in \mathbb{R}^{C \times H \times W}$ as input, which is obtained from the segmentation network as described in the previous section, the backbone network outputs the feature map $E^{(i)} \in \mathbb{R}^{C' \times H' \times W'}$. Mathematically,

$$E^{(i)} = f(x^{(i)}; \theta^{(1)}) \tag{1}$$

where $\theta^{(1)}$ denotes all the parameters of the backbone network, C denotes the number of channels of the input image ($C = 3$ for coloured images), H denotes the height of the image, W denotes the width of the image. Similarly, C',

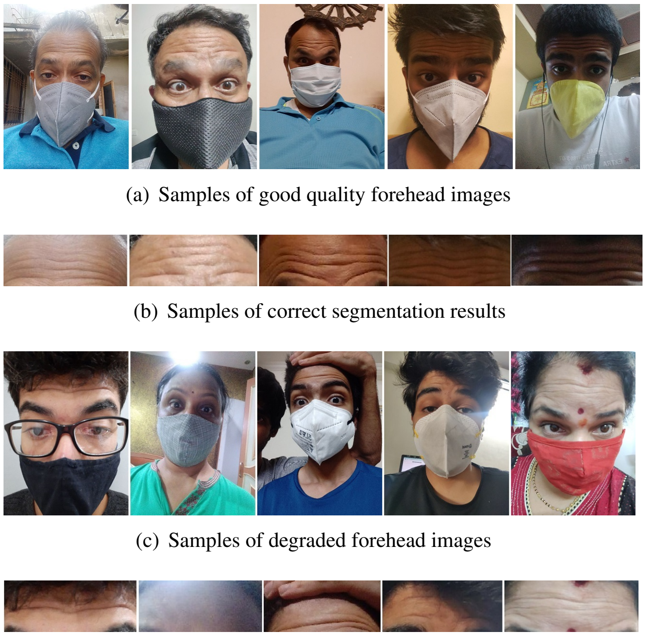

(a) Samples of good quality forehead images

(b) Samples of correct segmentation results

(c) Samples of degraded forehead images

(d) Samples of incorrect segmentation results

Figure 6: Masked face and corresponding forehead RoI using the segmentation network.

H', W' denotes the number of channels, height and width of the feature maps respectively. Since our in-house dataset is relatively small, we decided to use an efficient DNN which has comparatively less number of parameters so as to not overfit on the training data. Also to address the vanishing gradients problem, without any loss of generality, we have considered ResNet-18 [6] as our backbone network f, which is the simplest yet effective DNN architecture.

The number of parameters or the cardinality of the set $\theta^{(1)}$ comes out to be around 22 million. The feature map $E^{(i)}$ is extracted from the conv5_x layer of ResNet-18, and it is further passed as input to our dual attention sub module which is described in the next section.

3.3. Dual Attention Module (DAM)

In order to increase the discriminatory power and select leading forehead features, attention mechanism has been utilized to guide the network to automatically select regions that can most contribute to an accurate matching. Since forehead ROI's have a lot of background in the form of eyebrows, acne, hair and sometimes even makeup, it leads to distorted features and can reduce the discriminatory power. To ensure that the backbone network is not confused by such unimportant features and to only learn domain specific forehead patterns, we employ a dual attention module (DAM) mechanism to jointly model the inter-dependencies of spatial and channel level forehead features. DAM basically apply spatial attention module (SAM) and channel attention module (CAM) independently over the outputs of the last convolution layer of the backbone network.

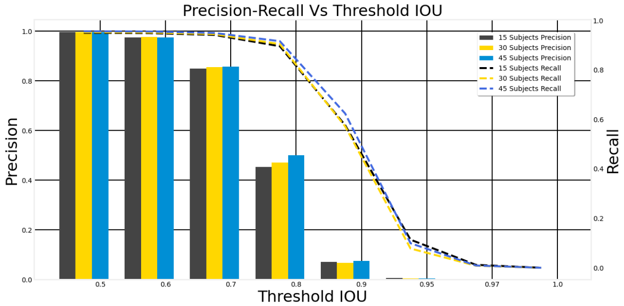

Figure 7: Precision/recall for different data sets w.r.t. IOU

The goal of spatial attention module is to aggregate the semantically similar pixels in the spatial domain of the input feature map. Though the spatial attention mechanism attends to the entire input feature map based on content (pixel values), it does not take into account the spatial positions of pixel.

Spatial Attention Module: Forehead images show plenty of spatial variations of lines and wrinkles that extends from one end of the image to the other. Spatial attention module (SAM) [4] allows us to capture the spatial semantic regularities present in the forehead patterns. Given the output feature map $E^{(i)}$ obtained from the backbone network, it is then passed through SAM to emphasize the spatial dependencies. This module can be represented as $A_{SAM}(E^{(i)};\theta^{(2)}) \in \mathbb{R}^{512\times7\times7}$, where $\theta^{(2)}$ denotes the weights of SAM module. Mathematically,

$$F_1^{(i)} = E^{(i)} \bigotimes A_{SAM}(E^{(i)};\theta^{(2)}) + E^{(i)} \qquad (2)$$

where $F_1^{(i)}$ is the final spatial highlighted features.

Channel Attention Module: To capture the channel-wise relationship of features obtained from the backbone network, it is of utmost importance to give higher significance to essential feature maps and thereby reducing prominence of redundant or unnecessary information. This further enables more stable training. To solve the same purpose, we deployed ECANet [20] as our channel attention module. This module can be implemented easily by 1D convolution of size F ($F = 5$) and only introduce a total of 6 training parameters. This module can be represented as $A_{CAM}(E^{(i)};\theta^{(3)}) \in \mathbb{R}^{512\times7\times7}$, where $\theta^{(3)}$ denotes the weights of CAM module. The output from this module is multiplied with the extracted feature map $E^{(i)}$ to get channel-wise highlighted features $F_2^{(i)}$ denoted as:

$$F_2^{(i)} = E^{(i)} \bigotimes A_{CAM}(E^{(i)};\theta^{(3)}) \qquad (3)$$

3.4. Feature Fusion

To effectively fuse the attention outputs obtained from CAM and SAM, we have considered the following two sce-

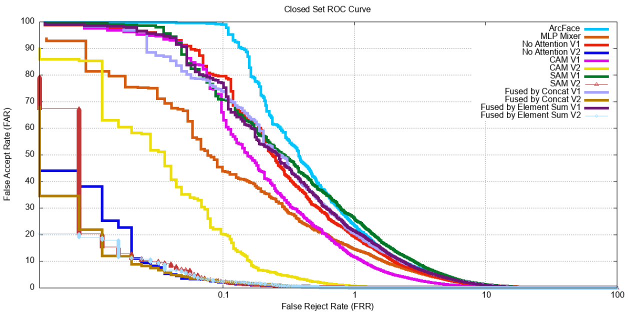

Figure 8: ROC Curves for the closed set experiments. The x-axis is shown in log scale.

narios.

First, we decided to concatenate the outputs obtained from the two attention modules. Mathematically,

$$O^{(i)} = F_1^{(i)} \| F_2^{(i)} \tag{4}$$

where $O^{(i)} \in \mathbb{R}^{2C' \times H' \times W'}$ is the feature map obtained after concatenating the two attention module outputs, and $\|$ denotes the concatenation operator.

Second, we performed an element wise addition between the two attention outputs. Mathematically,

$$O_j^{(i)} = {F_1}_j^{(i)} + {F_2}_j^{(i)} \tag{5}$$

where, ${F_1}_j^{(i)}$ is the j-th element of $F_1^{(i)}$, ${F_2}_j^{(i)}$ is the j-th element of $F_2^{(i)}$, $O_j^{(i)} \in \mathbb{R}^{C' \times H' \times W'}$ is the j-th element of output feature map. Thus, fusing the attention outputs from SAM and CAM, we can aggregate similar but less noticeable forehead wrinkle patterns to highlight their feature representation and can reduce the influence of saliant features like forehead skin, background, etc. The fused output O is then flattened to 1-dimension, passed into a fully-connected layer followed by a batch-normalization layer to obtain the final output feature vector $I^{(i)} \in \mathbb{R}^{512}$, which represents the embedding of the input forehead RoI image $x^{(i)}$. In this way, we have jointly model the spatial and channel-wise feature relationships and this process can be observed from Figure 3.

3.5. Loss Function and Network Training

Large margin cosine loss (LMCL) [19] is utilized for training the entire network in an end-to-end fashion. Training our model using this loss function results in learning features that are distinguishable in the cosine space. To have less intra-class variation (variation within same subject due to different poses, illumination, etc.) and more inter-class variations (variation between two different subjects), $m \geq 0$ is set as enforced margin so that features from different subjects are correctly matched. Given a set of two feature embeddings, the margin constrained can be defined as:

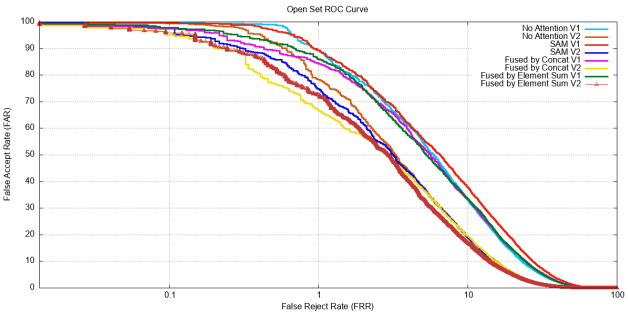

Figure 9: ROC Curves for the open set experiments. The x-axis is shown in log scale.

$$\cos\theta_1 - m > \cos\theta_2 \tag{6}$$

$$\cos\theta_2 - m > \cos\theta_1 \tag{7}$$

As our classification is binary, i.e. genuine and imposter. Eq 6 is the condition for matching within class 1 (genuine) and Eq 7 is the condition for matching within class 2 (impostor).Thus, based on margin constrained, the LMCL loss function can be formulated as:

$$L = \frac{1}{N}\sum_i -\log \frac{e^{s(\cos(\theta_{y_i}, i) - m)}}{e^{s(\cos(\theta_{y_i}, i) - m)} + \sum_{j \neq y_i} e^{s\cos(\theta_j, i)}} \tag{8}$$

where, $\cos(\theta_j, i) = W_j^T O^{(i)}$ and W_j is the weight vector of the j-th class.

Network training: Our dataset of 247 subjects was divided roughly equally into train and test set. We have set LMCL parameters $m = 0.35$, $s = 300$, and used feature embedding dimension as 512. The output obtained from LMCL is a vector of class probabilities. To facilitate backpropagation, output from LMCL is further passed to the focal loss [10] module with $\gamma = 2$. Additionally, the model weights are updated using adam optimizer [9], initial learning rate is set to $lr = 3 \times 10^{-4}$ and it is decayed by $\gamma = 0.1$ at every 20 epochs. We trained the network for 100 epochs with $L2$ weight penalty of $\lambda = 5 \times 10^{-4}$.

4. Experimental Results

In this section, matching protocols, ablation study, and comparative methods used for performance evaluation are described.

4.1. Matching Protocol

We used our trained model to evaluate various performance parameters to validate our approach. The images present in our train set are used as gallery, while the images present in the test set are used as query to perform matching. Each query image is matched with each one of

	Subject Count	Matching Strategy	CRR (%)	EER (%)	DI
Model V1	75	Open Set	96.08	17.50	1.44
Model V2	**75**	**Open Set**	**97.84**	**12.40**	**1.66**
Model V1	247	Closed Set	97.22	4.46	1.91
Model V2	**247**	**Closed Set**	**99.08**	**0.44**	**2.79**

Table 2: Closed Set and Open Set System performance on forehead dataset.

gallery images. During inference, the trained model is used to obtain the embeddings from gallery and query image set, and to match those embeddings. The embedding dimension is set to 512. Basically, a matching score is computed between a query and a gallery embedding by using L^2 (or the Euclidean) distance. A score between two embeddings is termed as **genuine matching** if they are obtained from same subjects, otherwise it is an **imposter matching**. We expect to see matching score for genuine matching to be very less, while matching score for imposter matching to be higher, because the learned metric distance is a measure of dissimilarity. In this task, we perform the following two kinds of matching experiments: closed set matching, and a hard matching strategy i.e., open set matching as described below.

Closed Set Matching: In this matching strategy, we consider all 247 subjects, and we divide the entire dataset almost equally into training (gallery) and testing set (query). So, we have 2462 images in gallery and 2502 images in query (one subject has more than 20 images).In this manner, we get 22768 genuine matchings and 5565663 imposter matchings. We evaluate matching performance on two kinds of models. First, **Model V1**, which is our proposed network trained on non-augmented dataset. Second, **Model V2**, which is our proposed network trained on augmented dataset.

Data Augmentation. For data augmentation, we sampled 5 points randomly from each of 45×45, 47×47, 49×49, and 51×51 neighbourhood around the center of the original bounding box of each ROI, and generated new ROI's using these sampled points as the center of the new bounding boxes, while keeping the height and width of the boxes unchanged. Thus, the dataset is augmented by 20 times which comes out to be $2462 \times 20 = 49,240$ images. However, it is important to note that the data augmentation process is done only for the training set and **Model V2** is then trained on augmented data.

Using the trained model's weights, we evaluated matching performance on our standard non-augmented dataset as described above. All the details about performance parameters such as correct recognition rate (CRR), equal error rate (EER), decidability index (DI) for the closed set matching can be observed from the Table 2. The respective ROC plots for this experiment is shown in Figure 8. On account of results, the following observations can be drawn: 1) Model V2 achieves the best individual performance in terms of both CRR (99.08%) and EER (0.44%). This is very good performance and it is getting close to iris [21], finger knuckle [8] biometrics systems. 2) Considering data augmentation, the network is allowed to see different variations of forehead patterns which drastically increases the generalisability of the network.

Model	Scenario	Subjects/ Poses	CRR %	EER %
V1 (No attention)	closed set	247	97.64	4.18
V2 (No attention)	closed set	247	99.36	0.38
V1 (No attention)	open set	75	96.92	17.06
V2 (No attention)	**open set**	**75**	**97.44**	**12.98**
V1 (Fused by Element Wise Sum)	open set	75	96.08	17.50
V2 (Fused by Element Wise Sum)	**open set**	**75**	**97.84**	**12.40**
V1 Fused by Concatenation	open set	75	95.52	17.45
V2 Fused by Concatenation	open set	75	97.71	13.22
V1 (SAM)	open set	75	93.43	19.19
V2 (SAM)	**open set**	**75**	**96.90**	**12.95**
V1 (SAM)	closed set	247	97.00	4.88
V2 (SAM)	closed set	247	99.32	0.39
V1 (CAM)	**closed set**	**247**	**98.10**	**3.02**
V2 (CAM)	closed set	247	99.48	0.90
V1 (Fused by Concatenation)	closed set	247	96.96	4.47
V2 (Fused by Concatenation)	closed set	247	99.24	0.48
V1 (Fused by Element Wise Sum)	closed set	247	97.22	4.46
V2 (Fused by Element Wise Sum)	**closed set**	**247**	**99.08**	**0.44**

Table 3: Ablation Study.

Open Set Matching: In this experiment, we consider a challenging matching strategy where 30% subjects are excluded from training. More specifically, our proposed model is first trained after removing 75 subjects from our dataset. Thus, the model is actually trained only on 172 subjects by splitting the dataset into training and testing sets equally. This trained model is then used to generate matching scores on the remaining unseen 75 subjects. In particular, all the images from the remaining unseen 75 subjects are split equally into gallery and query. Therefore, we consider 744 images in gallery and 742 images in query set. In this manner, a total of 7386 genuine matchings and 544662 imposter matchings are obtained. We again evaluate matching performance on two kinds of models: **Model V1** (trained on non-augmented dataset), and **Model V2** (trained on augmented dataset). The Data augmentation process remains same as described earlier. Only the training set images from 172 subjects are augmented, and the model V2 is trained on this augmented dataset. To evaluate the matching performance, the trained model's weights are used to generate matching scores on the remaining unseen 75 subjects. This unseen dataset is the same as used for Model V1. The performance parameters for the open set matching can be observed from the Table 2 and respective ROC plot can be seen from Figure. 9 On account of results, the following necessary observations can be realised: 1) Model V2 has better performance than Model V1 in both CRR(97.84% vs 96.08%) and EER (12.40% vs 17.50%) which justifies the importance of doing data augmentation. 2) Despite the challenging nature of open set matching, our model V2 still manages to improve EER on augmented data compared to model V1 which signifies the strength of our network.

In overall, it is evident from Table 2, that performance on

Approach	Dataset Statistics	Testing Protocol	CRR %	EER %
ResNet18 (Work by [11])	30 Subjects, 270 images	Validation Accuracy	94.47	NA
ResNet101 (Work by [11])	30 Subjects, 270 images	Validation Accuracy	98.55	NA
MLP Mixer [18] (Our Work)	247 Subjects, 4964 images	Standard Matching	92.31	4.08
ArcFace Loss [3] (Our Work)	247 Subjects, 4964 images	Standard Matching	97.47	4.54
Proposed (element sum fusion)	247 Subjects, 4964 images	Standard Matching	97.22	4.46
Proposed (concat fusion)	247 Subjects, 4964 images	Standard Matching	96.96	4.47
Proposed (SAM only)	247 Subjects, 4964 images	Standard Matching	97.00	4.88
Proposed (CAM only)	247 Subjects, 4964 images	Standard Matching	98.10	3.02
Proposed (element sum fusion) *	247 Subjects, 4964 images	Standard Matching	99.08	0.44
Proposed (concat fusion) *	247 Subjects, 4964 images	Standard Matching	99.24	0.48
Proposed (SAM only) *	247 Subjects, 4964 images	Standard Matching	99.32	0.39
Proposed (CAM only) *	247 Subjects, 4964 images	Standard Matching	99.48	0.90

Table 4: Comparison with other methods and settings. (* denotes model trained using augmented dataset.)

open set testing protocol gets deteriorated compared to the closed set results, but nevertheless, the CRR is very good, and it further increases our confidence on generalisability of our models on unseen datasets.

4.2. Ablation Study

In this section, we consider individual modules for the performance evaluation of our model architectures to have deeper understanding of bottleneck n/w and attention mechanisms. The model architectures i.e., Model V1 (non-augmented dataset) and Model V2 (augmented dataset) under various scenarios are considered and their matching results are shown in Table 3.

We first investigate how the attention criterion in terms of SAM and CAM independently affect the performance. Considering that forehead images are not that much complex and single attention mechanism might be sufficient to achieve the good performance and generalisability. Experiment results on open set matching, as shown in 6^{th} and 10^{th} rows of Table 3 describe that our model with dual attention achieves better performance in comparison to any of the individual attention blocks. However, in case of closed set matching, SAM shows comparable performance w.r.t. dual attention. From above two observations, it can be stated that dual attention mechanism provides more generalisability. The element wise sum operation in our DAM do the better joint learning of spatial and channel-wise features which justifies it's higher accuracy compared with the concatenation operation in both closed and open set matching protocols. On the other side, CAM reports best individual results (CRR: 98.10, EER: 3.02) on non-augmented data compared to *SAM* (CRR: 97.00, EER: 4.88). Conversely, when there is sufficient training data available or when we are using augmented dataset, we see the reverse trend and scenario *SAM* (CRR: 99.32, EER: 0.39) has the better performance because of its low EER as compared to *CAM* (CRR: 99.48, EER: 0.90). The *No Attention* scenario gives the best performance (CRR: 99.36, EER: 0.38) for augmented data as can be seen from 2^{nd} row in the case of closed set matching. However, the same scenario performs poorly (CRR: 97.44, EER: 12.98) in open set matching as shown in 4^{th} row of Table 3. Finally, one can conclude that to ensure model generalisability as well as higher performance, the use of dual attention based SAM and CAM, and combining the attention outputs according to Eq 4 gives us better results.

4.3. Comparative Analysis

To the best of our knowledge, this is the first work reporting forehead crease patterns for mobile based person recognition. The other paper [11] which is tangentially related to the scope of current study (already been discussed in previous sections) can't be directly compared due to following reasons: 1) authors have reported their results using k-fold cross validation, since they have not followed the standard matching protocol, there is no EER to report from their work. 2) authors have not reported any results on open set matching, and also the dataset used by them is not publicly available. Due to very less number of samples used in their experiments, the generalisability of their model can't be inferred. To make comparative analysis more significant, we have computed experimental results on our dataset by using other well known network architectures: MLP Mixer[18]; ArcFace loss[3]. From Table 4, one can observe that our models (Model V1, Model V2) trained using LMCL loss is performing better in all studied cases than the models trained using MLP Mixer and ArcFace.

5. Conclusion

This work investigates the usefulness of the forehead creases under surprised facial expression for smartphone based user recognition, hence very good potential as a biometric. In the COVID-19 situation when a person is mandated to wear face mask and not to touch surfaces, other biometric modalities such as face and fingerprint causes serious challenges. We device touch-less image acquisition using a mobile application and present a genealiszed deep learning framework with attention guided mechanism that further regularized using metric learning for better inter class variability. The system is evaluated on a masked face dataset acquired from 247 subjects that contains 4,964 selfie images. Our proposed network reports high performance results in open set and close set matching protocols: CRR: 99.08%, EER: 0.44% on closed set, and CRR: 97.84%, EER: 12.40% on open set experiments. These outperforming results are comparable to performance of iris, finger knuckle, and palmprint biometrics, and thus, validate our assumption for considering forehead creases as biometric modality to improve masked face scenarios.

References

[1] Tiago de Freitas Pereira and Séastien Marcel. Periocular biometrics in mobile environment. In *2015 IEEE 7th International Conference on Biometrics Theory, Applications and Systems (BTAS)*, pages 1–7. IEEE, 2015. 1

[2] Alexander De Luca, Alina Hang, Emanuel Von Zezschwitz, and Heinrich Hussmann. I feel like i'm taking selfies all day!

towards understanding biometric authentication on smartphones. In *Proceedings of the 33rd annual ACM conference on human factors in computing systems*, pages 1411–1414, 2015. 1

[3] Jiankang Deng, Jia Guo, Niannan Xue, and Stefanos Zafeiriou. Arcface: Additive angular margin loss for deep face recognition. In *Proceedings of the IEEE/CVF Conference on Computer Vision and Pattern Recognition*, pages 4690–4699, 2019. 8

[4] Jun Fu, Jing Liu, Haijie Tian, Yong Li, Yongjun Bao, Zhiwei Fang, and Hanqing Lu. Dual attention network for scene segmentation. In *Proceedings of the IEEE/CVF Conference on Computer Vision and Pattern Recognition*, pages 3146–3154, 2019. 4, 5

[5] David Haws and Xiaodong Cui. Cyclegan bandwidth extension acoustic modeling for automatic speech recognition. In *ICASSP 2019-2019 IEEE International Conference on Acoustics, Speech and Signal Processing (ICASSP)*, pages 6780–6784. IEEE, 2019. 1

[6] Kaiming He, Xiangyu Zhang, Shaoqing Ren, and Jian Sun. Deep residual learning for image recognition. In *Proceedings of the IEEE conference on computer vision and pattern recognition*, pages 770–778, 2016. 5

[7] Gaurav Jaswal, Amit Kaul, and Ravinder Nath. Knuckle print biometrics and fusion schemes–overview, challenges, and solutions. *ACM Computing Surveys (CSUR)*, 49(2):1–46, 2016. 2

[8] Gaurav Jaswal, Aditya Nigam, and Ravinder Nath. Finger knuckle image based personal authentication using deepmatching. In *2017 IEEE international conference on identity, security and behavior analysis (ISBA)*, pages 1–8. IEEE, 2017. 7

[9] Diederik P Kingma and Jimmy Ba. Adam: A method for stochastic optimization. *arXiv preprint arXiv:1412.6980*, 2014. 6

[10] Tsung-Yi Lin, Priya Goyal, Ross Girshick, Kaiming He, and Piotr Dollár. Focal loss for dense object detection. In *Proceedings of the IEEE international conference on computer vision*, pages 2980–2988, 2017. 6

[11] Jirapong Manit, Luise Preuße, Achim Schweikard, and Floris Ernst. Human forehead recognition: a novel biometric modality based on near-infrared laser backscattering feature image using deep transfer learning. *IET Biometrics*, 9(1):31–37, 2019. 2, 8

[12] Jirapong Manit, Achim Schweikard, and Floris Ernst. Deep convolutional neural network approach for forehead tissue thickness estimation. *Current Directions in Biomedical Engineering*, 3(2):103–107, 2017. 2

[13] Aditya Nigam and Phalguni Gupta. Designing an accurate hand biometric based authentication system fusing finger knuckleprint and palmprint. *Neurocomputing*, 151:1120–1132, 2015. 2

[14] Joseph Redmon and Ali Farhadi. Yolov3: An incremental improvement. *arXiv preprint arXiv:1804.02767*, 2018. 4

[15] Rahim Saeidi, Ilkka Huhtakallio, and Paavo Alku. Analysis of face mask effect on speaker recognition. In *Interspeech*, pages 1800–1804, 2016. 1

[16] Lingxue Song, Dihong Gong, Zhifeng Li, Changsong Liu, and Wei Liu. Occlusion robust face recognition based on mask learning with pairwise differential siamese network. In *Proceedings of the IEEE/CVF International Conference on Computer Vision*, pages 773–782, 2019. 1

[17] Juan Tapia, Marta Gomez-Barrero, Rodrigo Lara, Andres Valenzuela, and Christoph Busch. Selfie periocular verification using an efficient super-resolution approach. *arXiv preprint arXiv:2102.08449*, 2021. 2

[18] Ilya Tolstikhin, Neil Houlsby, Alexander Kolesnikov, Lucas Beyer, Xiaohua Zhai, Thomas Unterthiner, Jessica Yung, Daniel Keysers, Jakob Uszkoreit, Mario Lucic, et al. Mlpmixer: An all-mlp architecture for vision. *arXiv preprint arXiv:2105.01601*, 2021. 8

[19] Hao Wang, Yitong Wang, Zheng Zhou, Xing Ji, Dihong Gong, Jingchao Zhou, Zhifeng Li, and Wei Liu. Cosface: Large margin cosine loss for deep face recognition. In *Proceedings of the IEEE conference on computer vision and pattern recognition*, pages 5265–5274, 2018. 4, 6

[20] Qilong Wang, Banggu Wu, Pengfei Zhu, Peihua Li, Wangmeng Zuo, and Qinghua Hu. Eca-net: efficient channel attention for deep convolutional neural networks, 2020 ieee. In *CVF Conference on Computer Vision and Pattern Recognition (CVPR). IEEE*, 2020. 4, 5

[21] Zijing Zhao and Ajay Kumar. Towards more accurate iris recognition using deeply learned spatially corresponding features. In *Proceedings of the IEEE international conference on computer vision*, pages 3809–3818, 2017. 7